



## Effect of Ni-doping Charge on Structure and Properties of LiNbO<sub>3</sub>

A. El Bachiri <sup>a,\*</sup>, M. El Hasnaoui <sup>b</sup>, F. Bennani <sup>a</sup>, M. Bousselamti <sup>a</sup>

<sup>a</sup> Laboratory of Condensed Matter Physics, Department of Physics, Faculty of Sciences, Ibn Tofail University, BP: 133, 14 000 Kenitra, Morocco.

<sup>b</sup> LASTID Laboratory, Physics Department, Faculty of Sciences, Ibn-Tofail University, BP 133, Kenitra, Morocco.

Received 11 Apr 2016, Revised 04 Jun 2016, Accepted 09 Jun 2016

\*Corresponding author. E-mail: [bachiriabdo2009@hotmail.fr](mailto:bachiriabdo2009@hotmail.fr) (A. El Bachiri)

### Abstract

Phase formation and structural properties of Ni-doped Li<sub>0.976-x</sub>Nb<sub>1.005-x/5</sub>Ni<sub>x</sub>O<sub>3</sub> (0 ≤ x ≤ 0.1) ceramics prepared by solid-state reaction method, are investigated in a temperature range from 400 to 900 °C. X-ray diffraction patterns indicate that single phase was formed for lithium niobate ceramics. It was shown that the unit-cell volume of the hexagonal phase decreased with increasing nickel concentration from 0 to 3% Ni charge and increased above 3%. No secondary phases were observed in Ni-doped powder of LiNbO<sub>3</sub> for all concentrations compared with that of undoped sample. These results indicate that the Ni<sup>2+</sup> ion was substituted for niobium and lithium ions in the hexagonal phase. The addition of Ni<sup>2+</sup> promotes densification of lithium niobate ceramics. Raman spectra show that the samples were well crystallized with high purity. It was noticed that the increase of Ni-doping causes the decreasing of resistivity at high temperatures, but it has no influence of activation energy.

**Keywords:** Ceramics; Ni-doping charge; solid-state reaction; crystalline structure; electrical resistivity.

### 1. Introduction

Lithium niobate, LiNbO<sub>3</sub>, is a ferroelectric material well known for their technological applications in different fields. It has found use in the area of surface acoustic wave devices and capable of exhibiting a well defined domain structure. At room temperature, LiNbO<sub>3</sub> has a rhombohedral symmetry; its structure belongs to space group R3C and can be considered as a superstructure of the α-Al<sub>2</sub>O<sub>3</sub> corundum structure with Li<sup>+</sup> and Nb<sup>5+</sup> cations along the *c* axis [1]. Lithium niobate is well known to be narrow-range non-stoichiometric compounds; the solid solubility range extends from about 50 to 52% mol Nb<sub>2</sub>O<sub>5</sub> for lithium niobate [2]. According to the study reported by Abrahams *et al.* [3], ferroelectricity in this compound is due to the displacements of both the Nb and Li ions within the octahedric sites. Lithium niobate is in space group R3c and has a distorted perovskite-type structure below its Curie temperature (1210 °C). Planes of oxygen atoms are arranged in a distorted hexagonal close-packed arrangement, with the interstices alternately filled by lithium atoms, niobium atoms and vacancies. In a perfect crystal, each Li or Nb atom is surrounded by a distorted octahedron of O<sup>2-</sup> ions [4]. A representation of schematic projection of the unit cell of the polycrystalline structure of LiNbO<sub>3</sub> in the plane (001) has been done by Tatyana V. and Manfred W. [5].

Composite of doped LiNbO<sub>3</sub> have drawn much attention in recent years due to their potential applications including lasers, optical amplifiers, and integrated optical circuits [6-9]. To achieve the desired functionalities, various dopants are added to the system. For example, Fe doping is used for holographic storage and beam coupling [10], Nd is added for solid-state laser applications [11-14] and Mg is introduced to increase the resistance to photorefractive damage [15, 16]. In addition, dopant ions have also been employed as probes to investigate the structure of domain walls and defect/domain-wall interactions [17-19]. Torii *et al* [20] studied the evolution of T<sub>c</sub> (Curie temperature) as a function of doping in [Li<sub>1-x</sub>M<sup>2+</sup><sub>x/2</sub>Θ<sub>x/2</sub>]TaO<sub>3</sub> where Θ denote the vacancies and M=Zn, Ni, Mg and Ca. They showed that the change of the Curie temperature was found to be

closely related with the  $c/a$  ratio of the hexagonal cell. Recently, Mg-doped  $\text{LiNbO}_3$  ceramics has been prepared by polymeric precursor method [21], the analysis of Simões *et al.* [21] indicated that the pure and doped (with 1 mol% of Mg) of lithium niobate have good potentials for evaluation of their piezoelectric applications.

Our interest, in the present article, is to study the effect of Ni content on the structure and to evaluate the behavior of the resistivity, at different temperatures, for extracting information about the mechanism of charge transport of Ni/ $\text{LiNbO}_3$  ceramics prepared by the solid-state reaction method.

## 2. Experimental procedures

### 2.1. Materials and samples preparation

Ceramics  $\text{Li}_{0.976-x}\text{Nb}_{1.005-x/5}\text{Ni}_x\text{O}_3$  for  $x \in \{0; 0.01; 0.03; 0.05; 0.08; 0.1\}$  samples were prepared from solid-state reaction method by mixing the  $\text{Li}_2\text{CO}_3$ ,  $\text{Nb}_2\text{O}_5$  and  $\text{NiO}$  powders. The starting materials were high-purity  $\text{Li}_2\text{CO}_3$  (>99.9%) and  $\text{Nb}_2\text{O}_5$  (>99.9%). Lithium carbonate, niobium and nickel oxides were mixed by attrition with  $\text{ZrO}_2$  balls in the 1/3 balls, 1/3 isopropanol and 1/3 solid phase ratio and shaken for 12 h. After the sedimentation, the mixture was dried in a rot-vapor. The samples were fired in three steps of 10 h, with 400 °C, 600 °C and 800 °C. Powders were then isostatically pressed at 2500 bars to give pellets of 13 mm in diameter and 1 mm in thickness and were sintered at 1000 °C for 4 h with a heating rate of 100 °C/h.

### 2.2. Characterisation

In order to determine the composition of the studied materials, an analysis of cations was made using inductively coupled plasma-atomic emission spectroscopy (ICP-AES), in the central analysis unit of the CNRS in Vernaison (France). The structure, crystallinity and phase of the Ni-doped Lithium niobate ceramics were determined with a Philips PW 1729 diffractometer using the  $\text{CuK}$  wavelength. The surface morphology of the ceramics was characterized by scanning electron microscopy (SEM).

For the electrical measurement, the platinum electrodes were deposited on the pellet surface by painting. The painted pellets were placed in the oven at 700°C for 2 h to ensure the adhesion of the electrodes on the ceramic. The evolution of the resistivity was deduced by complex impedance spectroscopy. Isothermal measurements were carried out between 500 and 900°C. The instrumentation comprised a solatron-1260 Impedance Gain phase analyzer controlled by a PC computer. Applied voltage was fixed at 0.5 V.

## 3. Results and discussion

### 3.1. Crystal structure determination

The X-ray diffraction patterns of undoped and Ni-doped  $\text{LiNbO}_3$  with 1% and 10% ceramics synthesized are shown in Fig. 1. From the patterns it is clear that the ceramics are polycrystalline in nature. All peaks from the diffraction patterns are characteristic of pure  $\text{LiNbO}_3$ , suggesting that the incorporation of Ni into the material does not imply significant changes in the crystalline phase of  $\text{LiNbO}_3$ . The variation of the peaks intensity between the curves indicated the compositional inhomogeneity of the ceramics. As can be seen in Fig.1, the intensity of (012) peak apparent at  $2\theta=23.81^\circ$  decreased with increasing Ni composition. This suggests that  $\text{Ni}^{2+}$  substitutes  $\text{Li}^+$  and  $\text{Nb}^{5+}$  in the lattice. These observations are in good agreement with the results obtained by Simões *et al.* [21]. For  $\text{LiNbO}_3$  ceramic doped with magnesium prepared from polymeric precursor. The inter-planar spacing values  $d_{hkl}$  corresponding to the (104), (110), (006), (113), (202), (024), (116), (122), (018), (214) and (300) diffraction planes are summarized in Table 1, these values are compared with that of standard values of  $\text{LiMO}_3$  ( $M=\text{Nb}$  ou  $\text{Ta}$ ) compounds reported in similar structure [21, 22]. These results showed that the crystalline networks have a hexagonal structure which is in good agreement with our previous work on pure lithium niobate ceramics with different stoichiometry prepared by solid-state reaction method [22].

The cell parameters were determined from X-ray patterns recorded at scanning speed of  $1/4^\circ 2\theta/\text{min}$  and were refined by least square method calculations; they are reported in Table 2. When the Ni content increases from 0% to 3% mole, the volume cell decreases because the content of substitution of  $\text{Nb}_{\text{Li}}^{5+}$  ions by  $\text{Ni}^{2+}$  increases as can be seen in Table 3. As we know that the ionic radius of  $\text{Nb}^{5+}$  (64 pm) is slightly smaller than that of  $\text{Ni}^{2+}$  (69 pm), we should then observe an increase in the volume cell and not a decrease. But as the substitution of  $\text{Nb}^{5+}$  by  $\text{Ni}^{2+}$  is accompanied by decrease of vacancy in Li site to keep electrical neutrality of the material, the oxygen atoms forming the octahedron containing these ions have attracted by these cations  $\text{Li}^+$  and  $\text{Ni}^{2+}$ . Therefore, the small decreases in volume cell with increasing in Ni content, in the range from 5% to 10% mole Ni can be explained by the increase of vacancies in Nb sites (table 3).

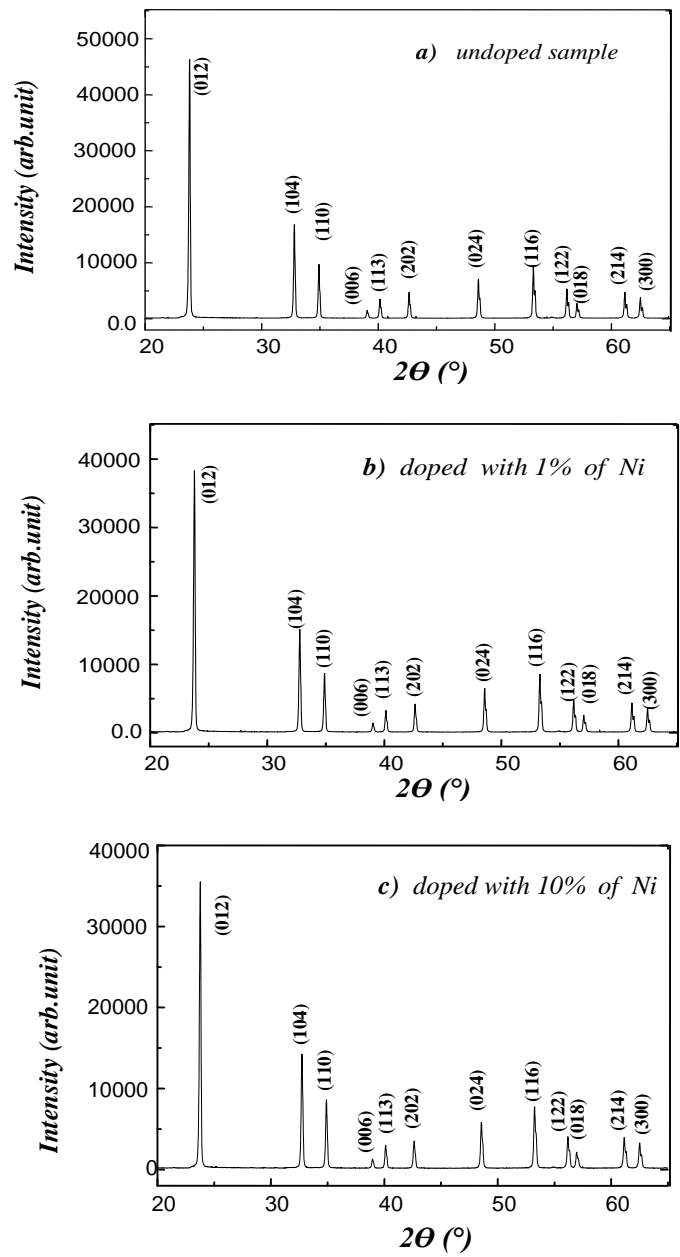


**Figure 1:** XRD patterns of samples, (a) undoped, (b) doped with 1% of Ni charge and (c) doped with 10% of Ni charge.

**Table 1:** Values of  $d_{hkl}$  of undoped and Ni-doped lithium niobate ceramics for different concentrations.

Samples Ni(%)	(012)	(110)	(006)	(113)	(202)	(024)	(116)	(122)	(018)	(240)	(300)
0	3.747	2.571	2.311	2.247	2.120	1.873	1.719	1.635	1.615	0.841	1.484
1	3.750	2.574	2.309	2.248	2.122	1.875	1.719	1.637	1.614	0.842	1.486
3	3.749	2.573	2.310	2.248	2.121	1.874	1.719	1.637	1.615	0.842	1.485
5	3.749	2.573	2.311	2.248	2.121	1.874	1.719	1.637	1.615	0.842	1.485
10	3.750	2.573	2.313	2.249	2.122	1.875	1.720	1.637	1.616	0.842	1.485

**Table 2:** Values of cell parameters for different concentrations of Ni-doped charge.

Samples Ni(%)	a(Å)	c(Å)	c/a	Volume Cell (Å <sup>3</sup> )
0	5.1425	13.8696	2.6970	318.89
1	5.1492	13.8597	2.6916	318.25
3	5.1472	13.8654	2.6938	318.20
5	5.1469	13.8714	2.6751	318.23
10	5.1475	13.8806	2.6965	318.53

Figures 2 (a) and (b), represent the variations of the cell parameters  $a_h$  and  $c_h$  with Ni-doping content, respectively. In regards to the parameter  $a_h$  is clearly observed the increase of this one parameter with Ni content from 0 to 1% mole Ni, followed by a slightly decrease in this lattice parameter from 3% to 10% at Ni, however the  $c_h$  parameter decreased for content lower than threshold of 1% moles of Ni, after this threshold the lattice parameter  $c_h$  increase with increasing Ni concentration. Similar results were found by S. Fang *et al* [23], in Zn-doped sample, and then these results seem logical since the cations in this structure are placed on the  $c_h$  axis.

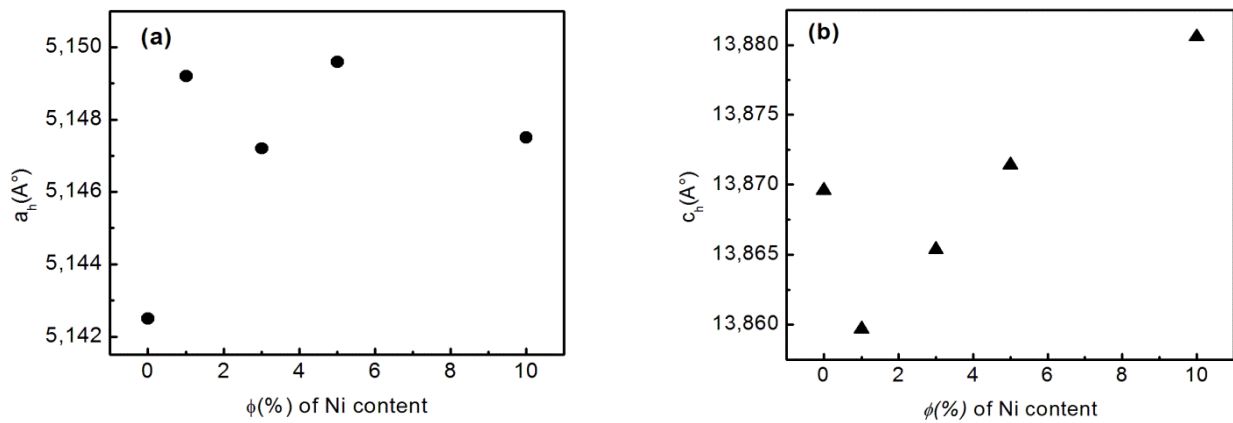


**Figure 2:** Lattice constants as a function of Ni-doped charge.

### 3.2. Surface morphology

Figure 3(a-b) shows typical SEM micrographs of the surface morphology of undoped and Ni-doped  $\text{LiNbO}_3$  with 3% of Ni. The grains are uniformly distributed throughout the surface of the sample showing its high compactness and polycrystallinity.

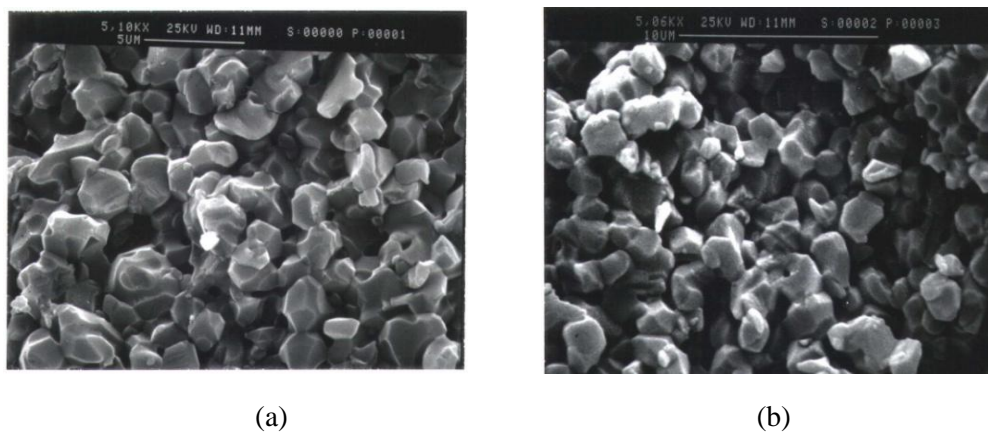


**Figure 3:** SEM micrographs of (a) un-doped sample and (b) Ni-doped sample with 3% of Ni charge.

The density of the ceramics was found to be around 89% compared with the theoretical density. The average grain size of compounds is between 2 and 3  $\mu\text{m}$  and the average grains size of Ni-doped lithium niobate is estimated from the X-ray diffraction patterns using the Scherrer formula [24], which is about 55 nm. The presence of voids of irregular dimensions indicates that the samples pellet has certain amount of porosity, the crystallites size difference found between SEM analysis and grains size in XRD diffraction can be explained by agglomeration of small grains to form large crystallites.

### 3.3. Composition analysis

The composition analysis of all samples was made by ICP-AES, in the central analysis unit of the CNRS in Vernaison, France. For a few compositions, we analyzed four samples of the same composition, to check the reliability of the analyses. The ICP-AES analysis reveals that the all samples contain lithium, niobium and nickel. The number of vacancies was calculated by subtraction of the amount of cation sites. Estimating errors in the formulas obtained are about 0.8% for Li, 0.1% for Nb and 0.5% for Ni. The formulas obtained are reported in Table 3. Taking into account the model described by Iyi *et al* [25] the prepared pure lithium niobate should have the chemical formula  $[\text{Li}_{0.976}\text{Nb}_{0.005}\Theta_{0.019}]\text{NbO}_3$  where  $\Theta$  denote the vacancies. When Ni cations are inserted in the lattice, it is thus probable that they are preferentially located on the lithium sites and replaced the niobium atoms. From the formulae given in Table 3, it is clear that the same results are obtained for a Ni content between 1 and 3%. For higher Ni contents, Ni cations should be located on both Li and Nb sites. For example, for  $x=0.05$  the formula should be  $[\text{Li}_{0.920}\text{Ni}_{0.046}\Theta_{0.034}][\text{Nb}_{0.996}\text{Ni}_{0.004}]\text{O}_3$ .

**Table 3:** Chemical formulae obtained by analysis and proposed formulae, where  $\Theta$  denote the vacancies.

Samples Ni(%)	Proposed formulae	Obtained formulae
0	$[\text{Li}_{0.976}\text{Nb}_{0.005}\Theta_{0.019}]\text{NbO}_3$	$\text{Li}_{0.976}\text{Nb}_{1.005}\text{O}_3$
1	$[\text{Li}_{0.96}\text{Nb}_{0.0038}\text{Ni}_{0.01}\Theta_{0.026}][\text{Nb}]\text{O}_3$	$\text{Li}_{0.960}\text{Nb}_{1.0038}\text{Ni}_{0.010}\text{O}_3$
3	$[\text{Li}_{0.939}\text{Nb}_{0.03}\Theta_{0.031}][\text{Nb}]\text{O}_3$	$\text{Li}_{0.939}\text{Nb}_{1.0}\text{Ni}_{0.030}\text{O}_3$
5	$[\text{Li}_{0.920}\text{Ni}_{0.046}\Theta_{0.034}][\text{Nb}_{0.996}\text{Ni}_{0.004}]\text{O}_3$	$\text{Li}_{0.920}\text{Nb}_{0.9958}\text{Ni}_{0.04975}\text{O}_3$
8	$[\text{Li}_{0.869}\text{Ni}_{0.074}\Theta_{0.057}][\text{Nb}_{0.9941}\text{Ni}_{0.006}]\text{O}_3$	$\text{Li}_{0.869}\text{Nb}_{0.9941}\text{Ni}_{0.08}\text{O}_3$
10	$[\text{Li}_{0.867}\text{Ni}_{0.086}\Theta_{0.047}][\text{Nb}_{0.988}\text{Ni}_{0.012}]\text{O}_3$	$\text{Li}_{0.867}\text{Nb}_{0.988}\text{Ni}_{0.098}\text{O}_3$

### 3.4. Raman spectroscopy

Raman spectroscopy is used to determine the structure, crystallinity and phases of our samples. The lithium niobate oxide crystallizes in the hexagonal structure, in which the  $\text{Li}^+$  ions occupy the 1/3 ed a sites and  $\text{Nb}^{5+}$  ions occupy the octahedral 1/3 ed sites.

The primitive unit cell of lithium niobate contains two formula weights (10 atoms), giving 30 degrees of freedom. Of these, 27 are assigned to optical phonon modes, with the other three as acoustic phonons [26]. Using group theory, the irreducible representations of optical modes of lithium niobate ( $R3c$  space group) are found to be [27].

$$\Gamma = 4A_1(Z) + 9E(X) + 9E(Y) + 5A_2 \quad (1)$$

The  $E$  modes are doubly degenerate, thus 27 modes are found, as expected. As only the  $A_1$  and  $E$  modes are Raman active, it may be expected to find a total of only 13 phonon peaks. Figure 4 shows Raman spectra of niobate oxide ceramics with different Ni contents, at room temperature. As it can be observed the samples doped with Ni show 13 well defined Raman peaks located at 152.5, 181, 238, 255.5, 275, 300, 320.5, 333, 368.5, 432, 581, 629.5 and 876.6  $\text{cm}^{-1}$  which correspond to modes of crystalline of  $\text{LiNbO}_3$  [27] in agreement with the group theory. This indicates that the as prepared samples consist of a single phase ( $\text{LiNbO}_3$ ), confirming the X-ray diffraction measurements. Small changes in the positions of several of the Raman peaks

were readily observed of the lithium niobate doped with Ni. All (FWHM) of Raman peaks changed when the content of doping increases, for example the value of (FWHM) for the peak located at  $152.5\text{ cm}^{-1}$ , is  $13.4\text{ cm}^{-1}$  for un-doped sample and  $11.9\text{ cm}^{-1}$  for sample doped with 5%Ni, this peak correspond to the E ( $\text{TO}_1$ ) mode assigned to the Nb-O vibration [27]. When Ni dopant concentration in lithium niobate was higher than threshold 3% Ni, all  $\text{Nb}_{\text{Li}}$  anti-sites were replaced completely, which decreased the content of the vacancy of Nb, this causes a scheduling of the Nb site and therefore a decrease in (FWHM). The (FWHM) of the mode  $\text{A}_1$  ( $\text{TO}_1$ ) increases, while its frequency is almost constant reflecting an increase in disorder on this site Nb and decreased the site of Li (mode  $\text{A}_1$  ( $\text{TO}_2$ ) Li-O vibration-related). Ni-dopant continues to replace the Nb in anti-sites  $\text{Nb}_{\text{Li}}$  but the compensation of the charge is essentially made by an increase in vacancies on the Nb site. These results are in good agreement with the XRD measurements.

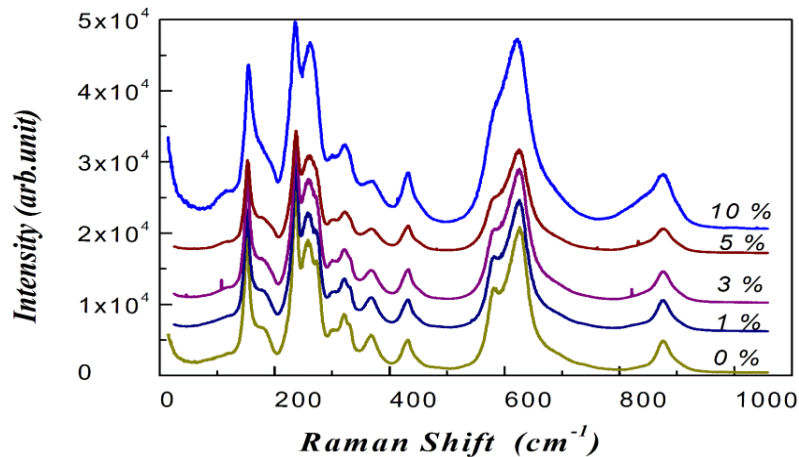


**Figure 4:** Raman spectra of lithium niobate oxide for different content of Ni-doped charge.

### 3.5. Electrical resistivity analysis

In order to examine the influence of Ni doping on resistivity of our samples we have represented, at different temperatures, its evolution with Ni content in Figure 5. From this figure two different behaviors can be seen. For the temperatures below  $700\text{ }^\circ\text{C}$  the variation of resistivity as a function of Ni content has no significant change, similar to the results of Brands and co-workers [28] who reported a study of iron-doped lithium niobate crystals, they found that the conductivity does not depend on iron concentration in the range of temperature ( $350 - 700^\circ\text{C}$ ), this behavior may be due to the band gap is too large for thermal excitation of electron hole-pairs. For the temperatures above  $700^\circ\text{C}$ , It is clear that the resistivity decreases with increasing of Ni charge, this behavior can be mainly attributed to effects of grouping of point defects; the same behavior was found also for other oxides [29]. The formation of these grouping of point defects was attributed to interactions electrostatic vacancy-doping.

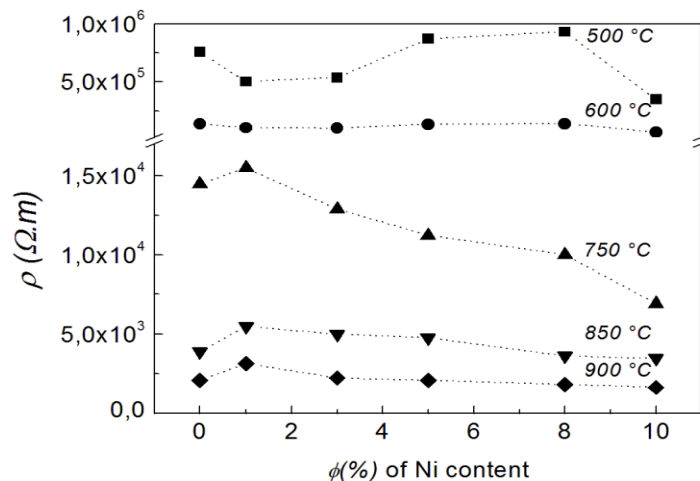


**Figure 5:** Electrical resistivity as a function of Ni-doped charge for different temperature.

Figure 6 shows the evolutions of the resistivity with temperature, for different content of Ni, it appears that the resistivity reveals a steadily decreasing behavior due to an increase charge mobility as temperature increases indicating that the mechanism result from thermally activated charge interactions which related to a cooperative effect of network modifiers ions mesostructure. Because the mobile charge ions in the mixed ceramic create a polarization system by reorienting locally, and are also responsible for conduction by separating itself from the immediate neighborhood [23]. Figure 7 shows the logarithms of electrical resistivity as a function of the inverse of temperature.

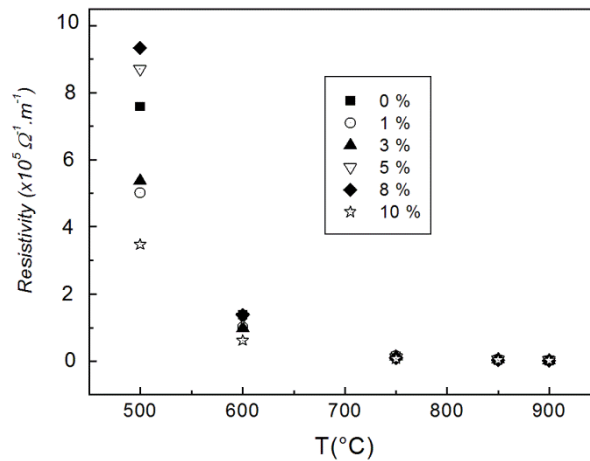


**Figure 6:** Electrical resistivity vs. temperature for different concentrations of Ni-doped charge.

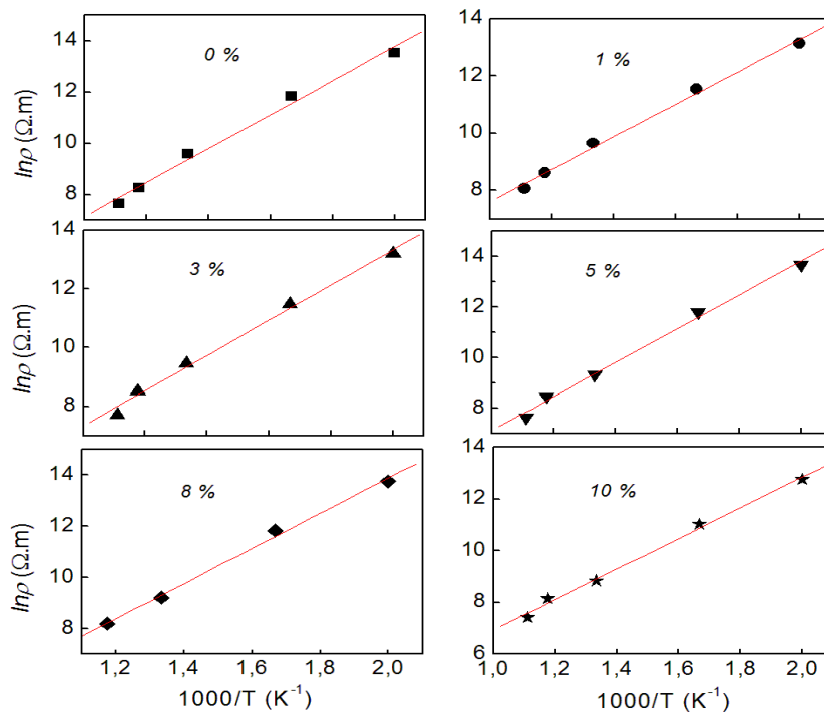


**Figure 7:** Arrhenius representation of resistivity for different concentrations of Ni-doped charge. The solid lines are the least square linear fits to Arrhenius relation.

It is clear from this figure that, the temperature dependence of resistivity typically follows the Arrhenius law:

$$\rho(T) = \rho_o \exp\left(\frac{W_a}{k_B * T}\right) \quad (2)$$

where  $\rho_o$  is the pre-exponential constant and  $k_B$  is the Boltzmann's constant.  $W_a$  is directly related to activation energy. The values of  $W_a$  and their correlation coefficients are resumed in Table 4.

**Table 4:** Values of activation energy for different Ni-doped LiNbO<sub>3</sub> samples using the Arrhenius equation.

Samples Ni(%)	0	1	3	5	8	10
$W_a$ (eV)	0.57	0.49	0.52	0.57	0.59	0.51
$R^2$	0.995	0.997	0.996	0.997	0.997	0.997

Note:  $R^2$  represents the correlation coefficient.

The activation energies obtained have no significant change with variation of Ni content and was found to be in the range from 0.49 to 0.59 eV with high correlation coefficients. These results show the same behavior with that obtained from Bennani *et al* [30] who have studied the effect of Ni charge on lithium tantalate. They found that these values are characteristics for ionic conduction due to the Li<sup>+</sup> cations. In doped lithium niobate the diffusion of Li<sup>+</sup> cations increases with the vacancy content. With excess of lithium, the diffusion of Li<sup>+</sup> cation is enhanced suggesting that the absence of difference in the activation energy for the different investigated samples is an indication of the dynamical of charge within the composite, where the charge interact weakly with the chain of the cristallin network. Furthermore, it helps to understand that there is a poor bond between the inserted charges and the crystalline molecular structure.

## Conclusion

Undoped and Ni-doped lithium niobate ceramics have been prepared by the conventional solid-state reaction method. The structural and electrical properties of these ceramics have been investigated as function of Ni content. The X-ray diffraction study showed that all the samples of undoped and Ni-doped lithium niobate were well crystallized and have polycrystalline hexagonal structure. X-ray diffraction analysis showed that Nickel charge has an influence on structure and electric properties of lithium niobate.

The results show that with the increase in Ni-doped content, the electrical resistivity decrease, which could be attributed to the increase in concentration. The high temperature resistivity dependence follows well the Arrhenius law for all compounds. This can be an indication of a certain dynamical of charge within the material as assumed in the literature.

## References:

1. Abrahams S.C., Bernstein J.L., *J. Phys. Chem. Sol.* 28 (1967) 1685–1692.
2. Boffi P., Piccinin D., Ubaldi M.C., *Infrared Holography for Optical Communications*, vol. 86, Springer, Berlin (2003).
3. Abrahams S.C., Keve E.T., *Ferroelectrics* 2 (1971)129-154.
4. Weis R.S., Gaylord T.K., *Appl. Phys. A* 37(1985) 191-203
5. Tatyana V., Manfred W., *Lithium Niobate: Defects, Photorefraction and Ferroelectric Switching*, Vol. 115, Springer, Berlin (2008).
6. Balsamo S., Maio S., Montrosset I., Suche H., Sohler W.,*Opt. Quantum Electron* 31(1999) 29-33.
7. Baumann I., Bosso S., Brinkmann R., Corsini R., Dinand M., Greiner A., Schafer K., Sochtig J., Sohler W., Suche H., Wessel R., *IEEE J. Sel. Top. Quantum Electron.* 2 (1996) 355-366.
8. Amin J., Aust J.A., Veasey D.L., Sanford N.A., *Electron. Lett.* 34 (1998) 456-459.
9. Voinot V., Ferriere R., Goedgebuer J.P., *Electron. Lett.* 34 (1998) 549-550.
10. Staebler D.L., Phillips W., *Appl. Opt.* 13 (1974) 788-794.
11. Lallier E., *Appl. Opt.* 31 (1992) 5276-5282.

12. Lallier E., Pocholle J.P., Papuchon M., Grezesbesset C., Pelletier E., Demicheli M., Li M.J., He Q., Ostrowsky D.B., *Electron. Lett.* 25 (1989) 1491-1492.
13. Johnson L.F., Ballman A.A., *J. Appl. Phys.* 40 (1969) 297-302.
14. Field S.J., Hanna D.C., Shepherd D.P., Tropper A.C., Chandler P.J., Townsend P.D., Zhang L., *Opt. Lett.* 16 (1991) 481-483.
15. Mouras R., Fontana M.D., Bourson P., Postnikov A.V., *J. Phys.: Condens. Matter.* 12 (2000) 5053-5059.
16. Bryan D.A., Gerson R., Tomaschke H.E., *Appl. Phys. Lett.* 44 (1984) 847-849.
17. Dierolf V., Morgus T., Sandmann C., Cantelar E., Cusso F., Capek P., Spirkova J., Polgar K., Sohler W., Ostendorf A., *Radiat. Eff. Defects Sol.* 158 (2003) 263-267.
18. Dierolf V., Sandmann C., Kim S., Gopalan V., Polgar K., *J. Appl. Phys.* 93 (2003) 2295-2297.
19. Dierolf V., Sandmann C., Gopalan V., Kim S., Polgar K., *Radiat. Eff. Defects Sol.* 158 (2003) 247-250.
20. Torii Y., Sekiya T., Yamamoto T., Kei Koyabachi, Yoshihiro Abe, *Mat. Res. Bull.* 18 (1983) 1569-1574.
21. Simões A.Z., Gonzalez A.H.M., Cavalheiro A.A., Zaghete M.A., Stojanovic B.D., Varela J.A., *Ceram. Int.* 28 (2002) 265-270.
22. El Bachiri A., Bennani F., Bouselamti M., *J. Asian Ceram. Soc.* 4 (2016) 46-54.
23. Fang S., Wang B., Zhang T., Ling F., Zhao Y., *Mater. Chemis. Physi.* 89 (2005) 249-252.
24. Kadam L., Patil P., *Mater. Chem. Phys.* 68 (2001) 225-232.
25. Iyi N., Kitamura K., Yajima Y., Kimura S., Furukawa Y., Sato M., *J. Sol. State Chem.* 118 (1995) 148-152.
26. Kittel C., *Introduction to Solid State Physics*, Wiley, New York (1996).
27. Repelin Y., Husson E., Bennani F., Proust C., *J. Phys. Chem. Sol.* 60 (1999) 819-825.
28. Brands K., Falki M., Haertle D., Woike T., Buse K., *Appl. Phys. B* 91 (2008) 279-281.
29. Steele D., Fender B.E.F., *J. Phys. C* 7 (1974) 1-11.
30. Bennani F., Husson E., *J. Europ. Ceramic Society* 21 (2001) 847-854.

(2016) ; <http://www.jmaterenvirosci.com/>